Engineering Thermostability in Artificial Metalloenzymes to Increase Catalytic Activity

Doble, Megan; Obrecht, Lorenz; Joosten, Henk-Jan; Lee, Misun; Rozeboom, Henriette J.; Branigan, Emma; Naismith, James H.; Janssen, Dick B.; Jarvis, Amanda G.; Kamer, Paul C. J.

Published in:
ACS Catalysis

DOI:
10.1021/acscatal.0c05413

Publication date:
2021

ACS Catalysis

pubs.acs.org/acscatalysis Research Article

Engineering Thermostability in Artificial Metalloenzymes to Increase Catalytic Activity

Megan V. Doble, Lorenz Obrecht, Henk-Jan Joosten, Misun Lee, Henriette J. Rozeboom, Emma Branigan, James. H. Naismith, Dick B. Janssen, Amanda G. Jarvis,* and Paul C. J. Kamer

Cite This: *ACS Catal.* 2021, 11, 3620–3627 Read Online

ACCESS | Metrics & More | Article Recommendations | Supporting Information

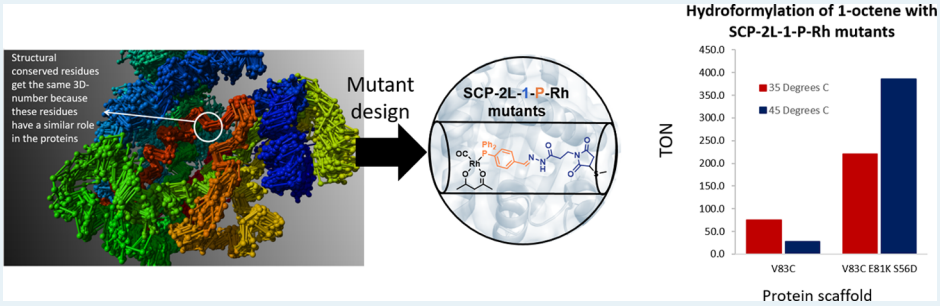

ABSTRACT: Protein engineering has shown widespread use in improving the industrial application of enzymes and broadening the conditions they are able to operate under by increasing their thermostability and solvent tolerance. Here, we show that protein engineering can be used to increase the thermostability of an artificial metalloenzyme. Thermostable variants of the human steroid carrier protein 2L, modified to bind a metal catalyst, were created by rational design using structural data and a 3DM database. These variants were tested to identify mutations that enhanced the stability of the protein scaffold, and a significant increase in melting temperature was observed with a number of modified metalloenzymes. The ability to withstand higher reaction temperatures resulted in an increased activity in the hydroformylation of 1-octene, with more than fivefold improvement in turnover number, whereas the selectivity for linear aldehyde remained high up to 80%.

KEYWORDS: *artificial metalloenzyme, hydroformylation, bioengineering, protein thermostability, biocatalysis, bioinformatics*

INTRODUCTION

Over the last decades, the power of biocatalysis in chemical synthesis, particularly within an industrial setting, has become undeniable. Enzymes such as transaminases and ketoreductases are increasingly used in the synthesis of chiral intermediates in pharmaceutical processes.[1−4] The use of biocatalytic technology to replace chemical steps as part of existing drug syntheses is attractive because of its simple nature and beneficial sustainability metrics.[5,6] The recent development of artificial metalloenzymes (ArMs) has added to the potential of biocatalysis by providing an elegant approach to combining enzymatic and chemical methods, thereby expanding the catalytic toolbox.[7−11] ArMs combine the molecular recognition properties of proteins, which are responsible for the high selectivity observed in many enzymatic processes, with the industrially relevant reactivity of homogeneous transition-metal catalysts. The introduction of synthetic transition-metal cofactors provides catalytic versatility by allowing unnatural reactions to be introduced into the biocatalysis arena. To date, a whole range of ArMs has been developed for unnatural reactions including transfer hydrogenation,[12] hydroformylation,[13,14] metathesis,[15] cross-coupling reactions,[16] and other carbon−carbon bond forming reactions such as the Diels−Alder reaction.[17−19] Nonetheless, the combination of proteins with organometallic catalysis remains challenging because of the different and contrasting conditions often required for efficient catalysis.[20] Proteins have evolved over time to work in a biological environment; therefore, harsh conditions, such as high temperatures and the presence of organic solvents favored in chemocatalysis, often lead to protein denaturation and deactivation of the catalyst.[21] Within the realm of biocatalysis, enzymes are nowadays routinely engineered to increase their stability to organic solvents and temperature, leading to more active enzymes.[22,23] One example showed that by using a computationally engineered variant with strongly improved thermostability, a peptide amidase could be applied in an organic solvent to achieve versatile peptide C-terminal

Received: December 9, 2020
Revised: February 23, 2021
Published: March 8, 2021

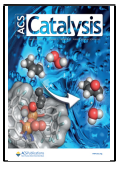

https://dx.doi.org/10.1021/acscatal.0c05413
ACS Catal. 2021, 11, 3620–3627

Scheme 1. Rhodium-Catalyzed Hydroformylation of Alkenes to Aldehyde Products

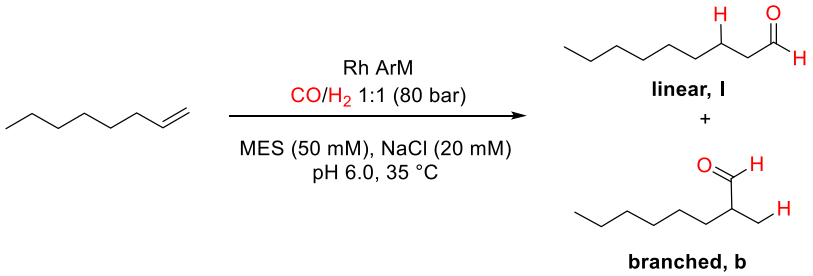

functionalization.[24] Based on such documented examples, we hypothesized that by enhancing the thermostability of the protein scaffold, it would be possible to increase the activity of ArMs and their tolerance to organic solvents.[25] This would expand the repertoire of possible reactions that ArMs could conduct and increase the experimental design space they can operate in.

A successful strategy used to engineer thermostability into a protein is the rational design of mutations based on structural information. Such mutations are focused on flexible regions in the protein, with the aim to reduce local unfolding.[26] Reduced flexibility can be achieved by a number of strategies including the introduction of disulfide bridges to stabilize early unfolding regions or destabilize the unfolded state by reducing its entropy.[27] Another strategy to enhance stability is the introduction of surface-located charged groups that can form salt bridges.[28] Such electrostatic interactions contribute to local stability, so it can be beneficial to introduce these into the flexible regions within the protein scaffold.[29] Several studies show that modifying other electrostatic interactions, such as the removal of isolated surface charges, also contributes to the stability of a protein.[30,31] Another approach to engineering thermostability employs phylogenetic or structure-based multiple sequence alignments to identify mutations and sequences that match the consensus sequence of a protein family. This approach is based on the hypothesis that the consensus amino acids (i.e., the most abundant amino acids at corresponding positions within a large set of aligned sequences or structures) generally add more to the stability of the protein than nonconsensus amino acids.[32]

The Kamer group has previously reported covalent approaches for synthesizing ArMs containing metal-binding ligands via a maleimide linker to unique cysteine residues in the protein scaffold human steroid carrier protein SL (SCP-2L).[33] The SCP-2L protein is a domain of 120 amino acids from the multifunctional enzyme type 2 (MFE-2, involved in β-oxidation) and was specifically selected for its ability to bind linear substrates in its hydrophobic tunnel.[34] Cysteine residues for protein modification were introduced at various locations within the tunnel, including V83C and A100C, to take advantage of substrate binding in the tunnel.[13,19] Hybrid catalysts based on these SCP-2L mutants in combination with phosphine-liganded Rh cofactors showed high activities and selectivities for the production of long-chain linear aldehydes in the rhodium-catalyzed hydroformylation of alkenes, under benign aqueous conditions (Scheme 1).[13] This reaction is of industrial interest because of the high added value of the aldehyde products in comparison to the alkene substrates. The catalyst performance is highly sensitive to the structure of the phosphine ligands, coordination number, and coordination mode.[35] Typically, highest selectivities for the desired linear aldehyde are obtained with two phosphine ligands coordinated in the equatorial plane of the trigonal bipyramidal RhH-$(CO)_2L_2$ catalyst resting state.[36] Monoligated complexes show generally much lower selectivities, and for ligand-free rhodium carbonyls, the linear-to-branched ratios go down to 1:1. In industry, rhodium-catalyzed hydroformylation is used on a large scale under biphasic conditions, enabling the recovery of the expensive rhodium catalyst. However, this reaction is challenging for longer alkenes (more than five carbon atoms) because of their low solubility under aqueous conditions.[37] ArMs provide a catalyst for longer alkene substrates that can work at low temperatures (<35 °C) compared to industrial conditions (typically 110−120 °C) and also offer high selectivity and turnover numbers (TONs), overall providing a much greener reaction. We set out to examine the use of sequence-based/rational protein engineering techniques to increase the stability of our artificial hydroformylase and thus increase the reaction temperature and the rate of hydroformylation.

RESULTS AND DISCUSSION

The design of mutations that could increase the stability of SCP-2L was carried out using both rational design and sequence-based mutant selection with an SCP-like family 3DM database.[38] The 3DM databases consist of structure-based alignments of homologous sequences and assign each residue a position number that allows comparison of positions among proteins that are structurally related within the protein family.[39] Both approaches require a 3D structure; therefore, we decided to solve the crystal structures of two variants that carry an introduced cysteine for the attachment of the artificial metal cofactor. The variants chosen were SCP-2L V83C and SCP-2L A100C which had been successfully used previously by the group in the development of hybrid catalysts for hydroformylation.[13] These mutants contained unique cysteines at either end of the hydrophobic tunnel for the introduction of the catalytic rhodium−phosphine complexes (Figure 1).

SCP-2L V83C and SCP-2L A100C were produced as previously described.[19] The structures of the two variants were determined by X-ray crystallography (see Supporting Information, pdb entries: 6Z1X and 6Z1W). The general fold of the wild-type SCP-2L with an α/β-fold consisting of five β-strands and five α-helices (PDB 1IKT)[34] is preserved; thus, the mutations lead to no structural change. The structural alignment between the variants and wild-type SCP-2L have a root-mean-square deviation of 0.3−0.5 Å over 115 aligned residues, with 99.1% sequence identity.

Both mutants contain Triton X-100, an analogue of a lipid molecule observed in the wild-type structure with similar interactions. The mutant V83C comprises two Triton X-100 molecules, with the (1,1,3,3-tetramethyl)butyl parts at ∼4.0 Å

https://dx.doi.org/10.1021/acscatal.0c05413
ACS Catal. 2021, 11, 3620−3627

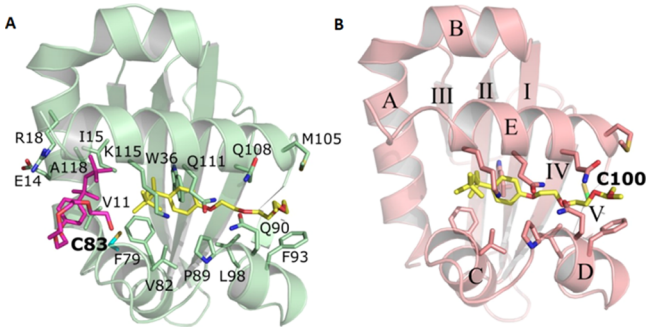

Figure 1. Crystal structures of the V83C (panel A, pdb: 6Z1X) and A100C (panel B, pdb: 6Z1W) mutants of SCP-2L; the ligand bound to the protein is Triton X-100 (2-[4-(2,4,4-trimethylpentan-2-yl)phenoxy]ethanol), shown as yellow or magenta sticks. The β-strands and α-helices are indicated by roman numerals (I–V) and capitals (A–E), respectively. The mutated residues are shown in cyan (structure A) and green (structure B).

from each other (Figure 1A). The second Triton X-100 has hydrophobic interactions with the side chains of V11, I15, C83, and A118 and with the hydrophobic part of the side chains of E14 and R18. The ethoxy repeats of Triton X-100 fold back into the SCP-2L molecule. The last ethoxy repeat visible in electron density has hydrophobic contacts with the phenyl group. The introduced C83 is situated on the C-terminal part of helix C, and the new C100 is in the middle of strand V (Figure 1B). The sulfur atom of C100 has hydrophobic contacts with one of the methyl groups of the butyl chain of the retained Triton X-100.

To stabilize the protein, we evaluated a number of mutation strategies, including stabilization of the flexible loop regions by salt bridge formation, strengthening of the α-helix dipoles, and mutations to introduce more conserved amino acids identified from the 3DM database alignments of the SCP-2L protein family. Stabilization by the introduction of disulfide bridges was avoided because of the requirement of a unique cysteine for the modification of the protein to introduce the metal cofactor and their incompatibility with phosphines.

Using the 3DM database and structural analysis of the protein, positions were identified where mutations toward consensus could be introduced without any expected loss of structural integrity (Figure 2). We excluded the four helices which surround the hydrophobic tunnel from mutagenesis because these are involved in the binding of ligands such as long-chain fatty acyl-CoAs[40] and cholesterol derivatives.[41] Mutations were especially sought in three loops that appear more flexible, as concluded from crystallographic B factors, which reflect the fluctuation of atoms from the average position because of protein dynamics.

Using the 3DM database, we found mutations that enable the introduction of more conserved residues within SCP-2L. Residue V26 is positioned within an α-helix and is 15.5% conserved in the SCP-like 3DM database (Figure S1). However, F26 is the more abundant residue in the whole protein family (27.5% conserved). The V26F mutation also introduces an aromatic group that could create π-stacking interactions. The following residues were also identified for mutation to more conserved residues: K40, G41, S54, and D116 (Table 1). Although the residue A68 is the most

Table 1. Effect of Designed Mutations on the Thermostability of SCP-2L V83C and A100C[a]

			template	
			A100C	V83C
entry	design method	mutation	$\Delta T_{m,app}$ (°C)	$\Delta T_{m,app}$ (°C)
1	stabilizing α-helix dipole	N31D	12	3
2	introducing a salt bridge	I44D	2	−1
3		I44E	4	1
4		S56D	11	10
5		S56E	−2	−7
6		K58D	5	np
7		K58E	u	1
8		K65D	np	np
9		K65E	7	1
10		E81K	9	6
11	toward consensus mutations	V26F	u	3
12		K40N	4	3
13		G41D	7	−6
14		S54N	np	np
15		A68P	3	4
16		D116K	2	0

[a]np, no data because of lack of protein; u, unreliable $T_{m,app}$ obtained.

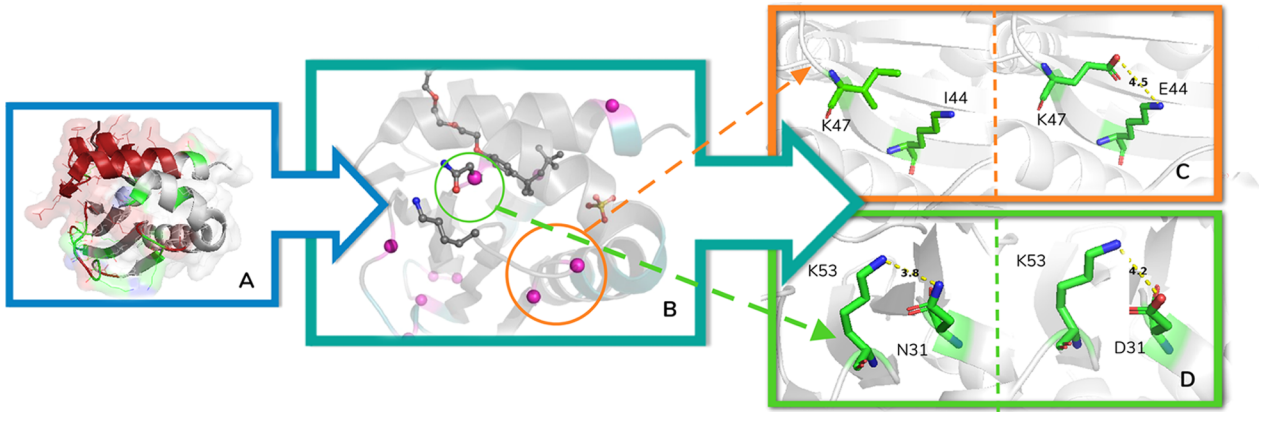

Figure 2. Position of mutations in SCP-2L (pdb 1IKT). (A) Positions and regions to be considered for mutagenesis are highlighted in green, and positions and regions to be avoided are indicated in red. (B) Positions of confirmed stabilizing mutations highlighted in pink spheres. (C) Introduction of a possible E44-K47 salt bridge by mutation I44E. (D) Introduction of a possible salt bridge K53-D31and strengthened dipole by mutation N31D. Image created in PyMOL.

https://dx.doi.org/10.1021/acscatal.0c05413
ACS Catal. 2021, 11, 3620−3627

conserved at 70%, proline is found in the same position for most of the remaining proteins (21%) and was thus also chosen as a conservative mutation.

We also explored the protein structure to identify residues that would lead to the formation of salt bridges that can stabilize flexible loops and regions on the protein surface. Residue I44 is positioned within a loop between β-sheets in a flexible region, and creating a salt bridge here was anticipated to increase the stability. It is also in close proximity to K47, and by introducing an E or D, an electrostatic interaction can be obtained (Figure 2C). Residues S56, K58, K65, and E81 were also identified as the sites for salt bridge formation, which can be achieved by reversing their charge to create new ionic interactions.

The alignment of the dipoles of peptide bonds parallel to the axis of an α-helix causes a net dipole moment with its positive pole at the amino terminus and negative pole at the carboxy terminus. The total dipole moment of the entire helix is due to the individual dipoles of the C═O groups involved in hydrogen bonding.[42] Phosphate moieties bind frequently at the positive N-termini of helices in proteins. Introducing a charged residue at the C-terminal positions can stabilize a helix by hydrogen-bonding to the main-chain CO group.[43] Residue N31 is present on the C-terminus of α-helix 1 of SCP-2L, with the side chain close to K53. To strengthen the interaction with the positively charged lysine, we introduced mutation N31D (Figure 2D). The stronger dipole and the formation of a new D31−K53 salt bridge were expected to increase the protein stability.

Site-directed mutagenesis[44] was performed both for SCP-2L A100C and V83C to separately obtain plasmids carrying the mutations G41D, S56D, K58E, K58D, I44E, I44D, E81K, S54N, S56E, D116K, I44D, K40N, A68P, K65E, N31D, or V26F (Table 1). All mutants were confirmed by DNA sequencing. Using circular dichroism (CD) spectroscopy, apparent melting temperature ($T_{m,app}$) values were measured[45] and compared with the parent proteins SCP-2L A100C and V83C (Figure S4). The CD method used a fast scan approach by measuring at six different temperatures. Reversibility was not established, and therefore the $T_{m,app}$ values are approximate as they can be influenced by incubation conditions; the values serve the purpose of indicating how the thermostability is affected by the mutations. The results showed that several mutants had a large improvement in thermostability over the original SCP-2L A100C and V83C proteins. The $T_{m,app}$ values increased by up to 12 and 10 °C for mutants constructed in A100C and V83C backgrounds, respectively. In general, the A100C protein template was more responsive to the designed mutations. The introduction of N31D gave an increase of 12 °C for A100C but only a 3 °C increase for V83C (Table 1, entry 1). The introduction of residues likely to form salt bridges raised the $T_{m,app}$ value of both mutants, with both E81K and S56D giving a large increase in $T_{m,app}$. The $T_{m,app}$ value of the mutant A100C increased by 9 and 11 °C for E81K and S56D, respectively, and with V83C, increases of 6 and 10 °C were observed (Table 1, entries 10, 4). Mutation S56D improved the $T_{m,app}$ value with both templates, whereas S56E led to a decrease in $T_{m,app}$ for both mutants. Introducing more conserved amino acids based on the results found using the 3DM database led to more modest increases in $T_{m,app}$. An exception was the G41D mutation in A100C which increased the $T_{m,app}$ value by 7 °C. In comparison, this mutation in V83C led to a decrease in $T_{m,app}$ by 6 °C (Table 1, entry 13).

There is ample evidence in the literature that combining mutations that increase thermostability can give an additive effect.[46] Therefore, the most favorable mutations from the first round of rational design (S56D, E81K, and N31D) were combined in different ways, and six double mutants were produced according to the same protocol as for the single mutants. Using CD spectroscopy, the melting temperature ($T_{m,app}$) of V83C and A100C and the thermostable double mutants were measured using data points taken with 1 °C intervals at 222 nm (Table 2 and Figure 3). This CD method provides a more accurate value than the fast scan approach used in the previous screen as a large number of data points are utilized.

Table 2. Apparent Melting Temperatures ($T_{m,app}$) of SCP-2L Mutants Determined Using CD, Measuring the Absorbance at 222 nm at 1 °C/min Steps

Variant	$T_{m,app}$ (°C)	ΔT (°C)
V83C template	48	
A100C template	42	
A100C + N31D + S56D	41	−1
A100C + N31D + E81K	55	+13
A100C + E81K + S56D	58	+16
V83C + N31D + S56D	60	+12
V83C + N31D + E81K	62	+14
V83C + E81K + S56D	64	+16

The designed double mutants showed impressive improvements in thermostability, increasing the $T_{m,app}$ value by 12−16 °C in all but one case (Table 2). Variant A100C + N31D + S56D revealed a negative effect of combining the N31D and S56D mutations and the $T_{m,app}$ value decreased by 1 °C. This protein was obtained in a very low yield (2 mg/L), so it was not used further in this work.

These results show that the rational design was successfully used to increase the stability of the SCP-2L-derived ArM protein hosts. Next, we examined if these stabilized scaffolds were suitable for creating more robust catalytic ArMs. Hydroformylation was chosen as a benchmark reaction because it is the most studied reaction using SCP-2L-derived ArMs. Previous results reported by the Kamer group showed that SCP-2L A100C and V83C rhodium proteins showed hydroformylation activity, reaching up to 400 and 100 TONs, respectively, over a 48 h reaction period.[13] These activities were surprisingly high, considering that the reactions were carried out at 35 °C. With a more stable protein scaffold, the activity might increase further as less catalyst degradation will occur over time allowing the use of higher temperatures.

The proteins were treated as previously described to give the phosphine-modified proteins, SCP2L X-**1**-**P**. Next, the rhodium metalloproteins for all five triple mutants (SCP-2L X variants with mutations X = A100C + N31D + E81K, A100C + E81K + S56D, V83C + N31D + E81K, V83C + E81K + S56D, or V83C + N31D + S56D) were obtained by the addition of $Rh(acac)(CO)_2$. The resulting proteins were analyzed by LC−MS to confirm the modification was effective (Scheme 2; see the Supporting Information for details).[33]

The hydroformylation activities of each of the five double mutants were investigated using 1-octene as the substrate and compared with SCP-2L A100C-**1**-**P**-**Rh** and V83C-**1**-**P**-**Rh** (Scheme 1). The reactions were carried out under the same conditions as the previous work, except for the reaction time,

https://dx.doi.org/10.1021/acscatal.0c05413
ACS Catal. 2021, 11, 3620−3627

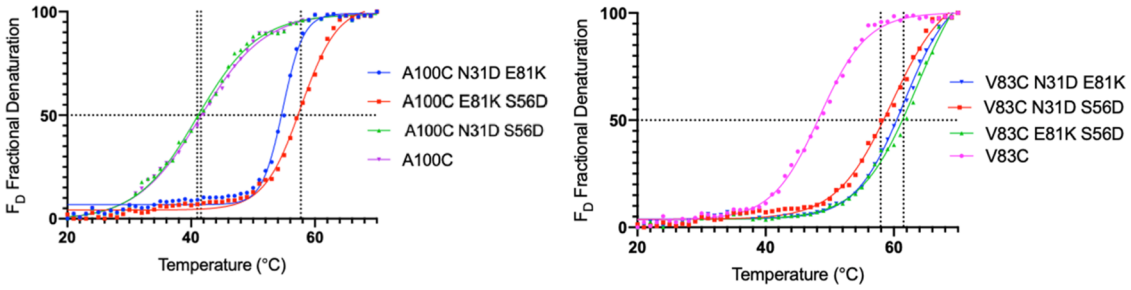

Figure 3. Thermal denaturation curves of SCP-2L double mutants.

Scheme 2. Synthesis of the Artificial SCP-2L-Derived Metalloproteins

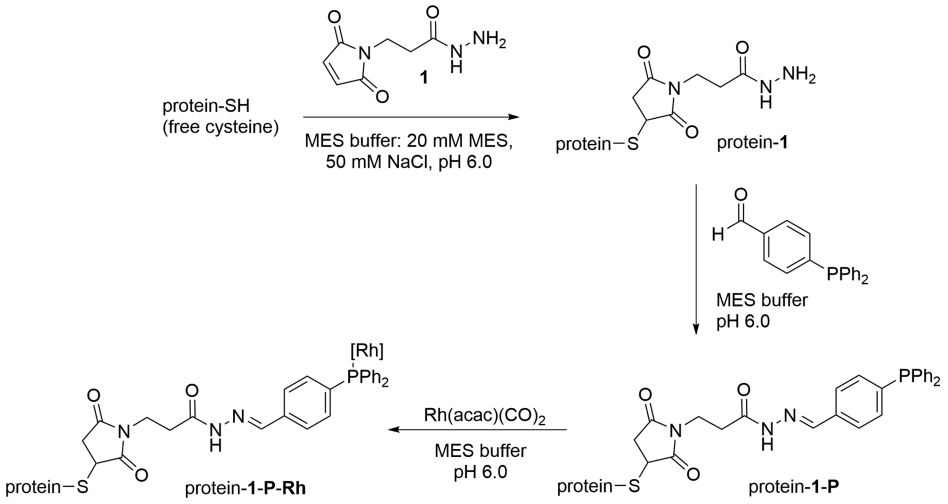

Table 3. Hydroformylation of 1-Octene Catalyzed by SCP-2L-Derived Rhodium Hydroformylases[a]

			16 h		48 h	
entry	mutant	temp °C	linear selectivity[b] (SD)	TON[c] (SD)	linear selectivity[b] (SD)	TON[c] (SD)
1	V83C	35	79 (0.2)	43 (0.3)	78 (1.2)	75.7 (1.3)
2		45	78 (0.1)	12 (1.3)	76 (1.0)	27.3 (1.0)
3	V83C + E81K + S56D	35	78 (0.1)	92 (1.0)	80 (0.7)	221 (1.9)
4		45	80 (0.1)	190 (1.1)	79 (0.9)	385 (3.9)
5	V83C + N31D + E81K	35	80 (0.1)	104 (0.9)	80 (1.1)	199 (2.0)
6		45	78 (0.3)	201 (0.9)	78 (0.7)	404 (4.2)
7	V83C + N31D + S56D	35	75 (0.1)	99 (1.0)	78 (1.9)	204 (2.8)
8		45	77 (0.1)	180 (1.2)	80 (0.8)	402 (4.3)
9	A100C	35	80 (0.1)	211 (0.7)	79 (0.8)	401 (3.9)
10		45	75 (0.2)	99 (2.9)	70 (1.6)	171 (2.7)
11	A100C + E81K + S56D	35	79 (0.7)	202 (1.3)	77 (1.2)	406 (5.2)
12		45	78 (1.1)	322 (3.1)	73 (0.9)	415 (3.9)
13	A100C + N31D + E81K	35	72 (0.2)	213 (0.4)	72 (1.3)	403 (3.5)
14		45	73 (0.5)	346 (2.1)	73 (1.3)	326 (2.8)
15	$Rh(acac)CO_2$ (no protein)[13]	35			55 (0.7)	530 (53)

[a]Conditions: 80 bar syngas (1:1), stirring 625 rpm, 16 h in degassed MES buffer, 0.5 mL of catalyst solution, and 0.5 mL of alkene containing 9% (v/v) *n*-heptane and 1% (v/v) diphenyl ether as internal standards. Results are the average of three repeated reactions, with standard deviation (SD) in brackets. Yields determined by GC. [b]Linear selectivity refers to the amount of linear aldehyde (%). [c]TON based on the Rh concentration of the catalyst solution, measured by ICP−MS.

which was shortened to 16 h (Table 3). Similar linear selectivities were observed as previously reported, and TONs were as expected for shorter reaction times (entries 1 and 9).[13] As seen previously, the use of the ArM gave higher linear selectivity (~80%) than just $Rh(acac)(CO)_2$, which exhibits only a slight preference for the linear aldehyde (Table 3, entry 15). The higher TON recorded for $Rh(acac)(CO)_2$ is consistent with Rh leaching into the organic layer in the absence of the phosphine-modified protein.

All three of the new thermostable SCP-2L V83C mutants (V83C + E81K + S56D, V83C + N31D + E81K, and V83C + N31D + S56D) showed an improvement in TONs compared to SCP-2L V83C at 35 °C. SCP-2L V83C E81K S56D gave a TON of 92 (TOF 6.5 h^{-1}), more than double that seen with

https://dx.doi.org/10.1021/acscatal.0c05413
ACS Catal. 2021, 11, 3620−3627

SCP-2L V83C under the same conditions (TON 43, TOF 2.9 h^{-1}, Table 3, entry 3 vs 1). This result, alongside the visual identification of the precipitated protein after the reaction with SCP-2L V83C only, suggests that significant denaturation occurred when using SCP-2L V83C as the protein scaffold and that increasing the thermostability of the scaffold protein increased the performance of the catalyst under these reaction conditions. Additional evidence was provided by comparing the CD spectra before and after the reaction. For V83C, an indistinct spectrum was obtained after the reaction, whereas for V83C + N31D + E81K, the far UV CD spectra still showed the expected features (see Supporting Information Figure S10 and S11). To test this further, the reaction temperature was increased to 45 °C, the hypothesis being that rates would increase at higher temperatures if the protein remains stable, and therefore a larger TON would be observed. For SCP-2L V83C (Table 3, entry 2) a significantly reduced TON was observed, most likely because of the rapid denaturation of the protein. However, the new thermostable rhodium-complexed proteins remained active at this higher temperature and produced high TONs of up to 200 (Table 3, entry 6), thus showing the expected increase in rate on increasing the temperature. The stabilized variants showed an approximate doubling of activity upon a 10 °C increase in reaction temperature, that is, for V83C + E81K + S56D, TOFs of 5.75 versus ∼11.9 h^{-1} were observed (Table 3 entry 3 vs 4; see Table S1 for data on TOF). For all V83C mutants, the selectivity toward the linear aldehyde remained high (75−80%) and thus provides evidence that the designed mutations did not interfere with the active sites of the catalysts.

The two new thermostable A100C-derived mutants (A100C + N31D + E81K and A100C + E81K + S56D) showed no improvement but consistent results with the parent A100C. However, when the reaction temperature was increased to 45 °C, these rhodium proteins were still stable, unlike the parent A100C, and showed increased TONs from 202 and 213 to 322 and 346 for A100C + E81K + S56D and A100C + N31D + E81K, respectively (Table 3, entries 11 vs 12 and 13 vs 14). This increase in TON is somewhat lower than what would be expected by increasing the reaction temperature by 10 °C, indicating that the newly designed A100C mutants are at the limit of their stability, which is also indicated by the relatively low increase in TON after longer reaction times (Table 3, entries 12 and 14). The linear selectivity of the catalysts was not significantly affected by the mutations, though a small decrease in selectivity was observed for A100C + N31D + E81K.

To test the long-term stability of the ArMs, the reaction time was further increased to 48 h to see if the TON could be improved (Table 3). As was seen after 16 h, the new thermostable V83C mutants showed an increase of TON from the original 76 of V83C up to 221 for V83C + E81K + S56D at 35 °C (Table 3, entries 1 and 3, respectively), representing an almost tripling of rate (TOF 1.6 vs 4.6 h^{-1}). When the temperature was raised to 45 °C, the TONs doubled for both V83C + N31D + E81K and V83C + N31D + S56D, giving rise to an expected increase in TOF from ∼4 h^{-1} to 8 h^{-1} (Table 3 entry 8; for TOFs, see Table S1). This suggests that the SCP-2L V83C-derived thermostable mutants are capable of retaining their structure at this higher temperature. However, comparing the average reaction rate over 16 and 48 h for all the V83C proteins, a drop of ∼30% over the second time frame is observed in all cases, regardless of the temperature. Thus, although thermostability has increased, some loss of activity during the reaction still occurs, potentially because of the exposure of the protein to mechanical stress through stirring and pressure.

In comparison to the C83 derivatives, the A100C-derived thermostable mutants showed less improvement in activity over the longer 48 h reaction period. This matched the observations from the 16 h reaction, which already implied that after 16 h the protein scaffold begins to denature, as shown by a large buildup of white precipitate. This indicates that inactivation is accompanied by aggregate formation and thus is irreversible. The loss of catalyst activity over the 48 h reaction period at 45 °C resulted in a drop of the average TOF for the A100C + N31D + E81K enzyme of almost 70%, that is, from 21.6 h^{-1} over a 16 h reaction to 6.8 h^{-1} for a 48 h reaction (Table 3, entry 14). This relatively large drop in activity does not appear to be related to thermostability as the mutations introduced in the C100 and C83 scaffolds gave similar $\Delta_{Tm,app}$ values. Instead, the loss of activity may be related to conversion, as the most active variants (Table 3, entries 12 and 14) show the largest reduction of activity.

Overall, the enhanced activity was correlated to the increase in stability of the SCP-2L-derived ArMs, as reflected in the $T_{m,app}$ values. All of the results show a high linear selectivity in hydroformylation reactions, indicating the catalysis occurs because of the artificial catalytic center introduced into the protein tunnel and not from "free Rh". Furthermore, the linearity of up to 80% remains very high for a monoligated Rh-catalyst, corroborating the importance of the second coordination sphere of the protein scaffold.[13]

CONCLUSIONS

In conclusion, we have shown that the stability of the protein scaffold within an ArM is a crucial factor with respect to the catalytic performance. Space−time yields are of crucial importance for industrial applications, especially when costly catalysts such as ArMs based on noble metals are concerned. The advantage of mild and green operating conditions of biocatalysts can be counterbalanced by low stability. By improving the thermostability of the SCP-2L V83C scaffold by up to 16 °C, we were able to increase the reactivity of our ArM at higher temperatures. With the stabilized hybrid enzymes, the TON improved over fivefold, reaching values of up to over 400. Although this study did not explore the increased solvent tolerance of the ArMs explicitly, the increased TON under biphasic conditions strongly indicates an increased stability in the presence of organic solvents. The increased organic solvent tolerance opens the door to study the reactions of substrates that need organic cosolvents for solubility. Thus, rational mutant design for improving ArM stability yielded a biocatalyst that enables a wider range of reaction conditions and showed higher activities. In addition to other powerful tools in biocatalysis and protein engineering, such as directed evolution, this may offer an attractive approach to tailor biocatalysts to fit real industrial applications.

ASSOCIATED CONTENT

Supporting Information

The Supporting Information is available free of charge at https://pubs.acs.org/doi/10.1021/acscatal.0c05413.

Experimental procedures, instrumental information, and product characterization (PDF)

https://dx.doi.org/10.1021/acscatal.0c05413
ACS Catal. 2021, 11, 3620−3627

AUTHOR INFORMATION

Corresponding Author

Amanda G. Jarvis − *School of Chemistry, University of St Andrews, KY16 9ST St Andrews, U.K.; School of Chemistry, University of Edinburgh, EH9 3FJ Edinburgh, U.K.;* orcid.org/0000-0002-6414-0497; Email: amanda.jarvis@ed.ac.uk

Authors

Megan V. Doble − *School of Chemistry, University of St Andrews, KY16 9ST St Andrews, U.K.*

Lorenz Obrecht − *School of Chemistry, University of St Andrews, KY16 9ST St Andrews, U.K.*

Henk-Jan Joosten − *Bio-Prodict, 6511 AA Nijmegen, The Netherlands*

Misun Lee − *Biotransformation and Biocatalysis, Groningen Biomolecular Sciences and Biotechnology Institute, University of Groningen, 9747 AG Groningen, The Netherlands*

Henriette J. Rozeboom − *Biotransformation and Biocatalysis, Groningen Biomolecular Sciences and Biotechnology Institute, University of Groningen, 9747 AG Groningen, The Netherlands*

Emma Branigan − *School of Chemistry, University of St Andrews, KY16 9ST St Andrews, U.K.*

James. H. Naismith − *School of Chemistry, University of St Andrews, KY16 9ST St Andrews, U.K.; Rosalind Franklin Institute, OX11 0FA Didcot, U.K.;* orcid.org/0000-0001-6744-5061

Dick B. Janssen − *Biotransformation and Biocatalysis, Groningen Biomolecular Sciences and Biotechnology Institute, University of Groningen, 9747 AG Groningen, The Netherlands;* orcid.org/0000-0002-0834-2043

[¶]Paul C. J. Kamer − *School of Chemistry, University of St Andrews, KY16 9ST St Andrews, U.K.; Bioinspired Homo- & Heterogeneous Catalysis, Leibniz Institute for Catalysis, Rostock 18059, Germany;* orcid.org/0000-0002-9115-8844

Complete contact information is available at: https://pubs.acs.org/10.1021/acscatal.0c05413

Funding

M.V.D thanks BBSRC for support through an EastBio studentship BB/J01446X/1. A.G.J. thanks the University of Edinburgh for support through a Christina Miller Fellowship and the EU for support through a Marie Curie Individual Fellowship, project ArtOxiZymes (H2020-MSCA−IF−2014-657755). The authors thank EPSRC for funding through the EPSRC critical mass grant "Clean catalysis for sustainable development" (EP/J018139/1). The UK Catalysis Hub is kindly thanked for resources and support provided via the authors' membership of the UK Catalysis Hub Consortium, which is funded by EPSRC (EP/K014706/2, EP/K014668/1, EP/K014854/1, EP/K014714/1, and EP/M013219/1).

Notes

The authors declare no competing financial interest.

[¶]Professor Paul Kamer passed away November 19, 2020.

ACKNOWLEDGMENTS

We thank Dr. T. Glumoff (University of Oulu, Finland) and Prof. Dr. K. J. Hellingwerf (University of Amsterdam) for providing plasmids. In addition, we thank the St Andrews Mass Spectrometry and Proteomics facility for help with the mass spectrometry instruments.

ABBREVIATIONS

ArM, artificial metalloenzyme; SCP-2L, sterol carrier protein type 2-like domain

REFERENCES

(1) Fuchs, M.; Farnberger, J. E.; Kroutil, W. The Industrial Age of Biocatalytic Transamination. *Eur. J. Org Chem.* **2015**, *2015*, 6965−6982.

(2) Patel, R. Biocatalytic Synthesis of Chiral Alcohols and Amino Acids for Development of Pharmaceuticals. *Biomolecules* **2013**, *3*, 741−777.

(3) Slabu, I.; Galman, J. L.; Lloyd, R. C.; Turner, N. J. Discovery, Engineering, and Synthetic Application of Transaminase Biocatalysts. *ACS Catal.* **2017**, *7*, 8263−8284.

(4) Moore, J. C.; Pollard, D. J.; Kosjek, B.; Devine, P. N. Advances in the Enzymatic Reduction of Ketones. *Acc. Chem. Res.* **2007**, *40*, 1412−1419.

(5) Savile, C. K.; Janey, J. M.; Mundorff, E. C.; Moore, J. C.; Tam, S.; Jarvis, W. R.; Colbeck, J. C.; Krebber, A.; Fleitz, F. J.; Brands, J.; Devine, P. N.; Huisman, G. W.; Hughes, G. J. Biocatalytic Asymmetric Synthesis of Chiral Amines from Ketones Applied to Sitagliptin Manufacture. *Science* **2010**, *329*, 305−309.

(6) Huffman, M. A.; Fryszkowska, A.; Alvizo, O.; Borra-Garske, M.; Campos, K. R.; Canada, K. A.; Devine, P. N.; Duan, D.; Forstater, J. H.; Grosser, S. T.; Halsey, H. M.; Hughes, G. J.; Jo, J.; Joyce, L. A.; Kolev, J. N.; Liang, J.; Maloney, K. M.; Mann, B. F.; Marshall, N. M.; McLaughlin, M.; Moore, J. C.; Murphy, G. S.; Nawrat, C. C.; Nazor, J.; Novick, S.; Patel, N. R.; Rodriguez-Granillo, A.; Robaire, S. A.; Sherer, E. C.; Truppo, M. D.; Whittaker, A. M.; Verma, D.; Xiao, L.; Xu, Y.; Yang, H. Design of an in vitro biocatalytic cascade for the manufacture of islatravir. *Science* **2019**, *366*, 1255−1259.

(7) Schwizer, F.; Okamoto, Y.; Heinisch, T.; Gu, Y.; Pellizzoni, M. M.; Lebrun, V.; Reuter, R.; Köhler, V.; Lewis, J. C.; Ward, T. R. Artificial Metalloenzymes: Reaction Scope and Optimization Strategies. *Chem. Rev.* **2018**, *118*, 142−231.

(8) Doble, M. V.; Ward, A. C. C.; Deuss, P. J.; Jarvis, A. G.; Kamer, P. C. J. Catalyst design in oxidation chemistry; from KMnO4 to artificial metalloenzymes. *Bioorg. Med. Chem.* **2014**, *22*, 5657−5677.

(9) Rosati, F.; Roelfes, G. Artificial Metalloenzymes. *ChemCatChem* **2010**, *2*, 916−927.

(10) Deuss, P. J.; den Heeten, R.; Laan, W.; Kamer, P. C. J. Bioinspired Catalyst Design and Artificial Metalloenzymes. *Chem.—Eur. J.* **2011**, *17*, 4680−4698.

(11) Heinisch, T.; Ward, T. R. Design strategies for the creation of artificial metalloenzymes. *Curr. Opin. Chem. Biol.* **2010**, *14*, 184−199.

(12) Dürrenberger, M.; Heinisch, T.; Wilson, Y. M.; Rossel, T.; Nogueira, E.; Knörr, L.; Mutschler, A.; Kersten, K.; Zimbron, M. J.; Pierron, J.; Schirmer, T.; Ward, T. R. Artificial Transfer Hydrogenases for the Enantioselective Reduction of Cyclic Imines. *Angew. Chem., Int. Ed.* **2011**, *50*, 3026−3029.

(13) Jarvis, A. G.; Obrecht, L.; Deuss, P. J.; Laan, W.; Gibson, E. K.; Wells, P. P.; Kamer, P. C. J. Enzyme Activity by Design: An Artificial Rhodium Hydroformylase for Linear Aldehydes. *Angew. Chem., Int. Ed.* **2017**, *129*, 13784−13788.

(14) Imam, H. T.; Jarvis, A. G.; Celorrio, V.; Baig, I.; Allen, C. C. R.; Marr, A. C.; Kamer, P. C. J. Catalytic and biophysical investigation of rhodium hydroformylase. *Catal. Sci. Technol.* **2019**, *9*, 6428−6437.

(15) Jeschek, M.; Reuter, R.; Heinisch, T.; Trindler, C.; Klehr, J.; Panke, S.; Ward, T. R. Directed evolution of artificial metalloenzymes for in vivo metathesis. *Nature* **2016**, *537*, 661−665.

(16) Chatterjee, A.; Mallin, H.; Klehr, J.; Vallapurackal, J.; Finke, A. D.; Vera, L.; Marsh, M.; Ward, T. R. An enantioselective artificial Suzukiase based on the biotin-streptavidin technology. *Chem. Sci.* **2016**, *7*, 673−677.

(17) Deuss, P. J.; Doble, M. V.; Jarvis, A. G.; Kamer, P. C. J. In *Artificial Metalloenzymes and MetalloDNAzymes in Catalysis: From Design to Applications*; Diéguez, M., Bäckvall, J.-E.; Pàmies, Eds.; Wiley, 2018; pp 285−319.
(18) Reetz, M. T. Artificial Metalloenzymes as Catalysts in Stereoselective Diels-Alder Reactions. *Chem. Rec.* **2012**, *12*, 391−406.
(19) Deuss, P. J.; Popa, G.; Slawin, A. M. Z.; Laan, W.; Kamer, P. C. J. Artificial Copper Enzymes for Asymmetric Diels-Alder Reactions. *ChemCatChem* **2013**, *5*, 1184−1191.
(20) Rudroff, F.; Mihovilovic, M. D.; Gröger, H.; Snajdrova, R.; Iding, H.; Bornscheuer, U. T. Opportunities and challenges for combining chemo- and biocatalysis. *Nat. Catal.* **2018**, *1*, 12−22.
(21) Musil, M.; Konegger, H.; Hon, J.; Bednar, D.; Damborsky, J. Computational Design of Stable and Soluble Biocatalysts. *ACS Catal.* **2019**, *9*, 1033−1054.
(22) Arabnejad, H.; Dal Lago, M.; Jekel, P. A.; Floor, R. J.; Thunnissen, A.-M. W. H.; Terwisscha van Scheltinga, A. C.; Wijma, H. J.; Janssen, D. B. A robust cosolvent-compatible halohydrin dehalogenase by computational library design. *Protein Eng. Des. Sel.* **2017**, *30*, 173−187.
(23) Cerdobbel, A.; De Winter, K.; Aerts, D.; Kuipers, R.; Joosten, H.-J.; Soetaert, W.; Desmet, T. Increasing the thermostability of sucrose phosphorylase by a combination of sequence- and structure-based mutagenesis. *Protein Eng. Des. Sel.* **2011**, *24*, 829−834.
(24) Wu, B.; Wijma, H. J.; Song, L.; Rozeboom, H. J.; Poloni, C.; Tian, Y.; Arif, M. I.; Nuijens, T.; Quaedflieg, P. J. L. M.; Szymanski, W.; Feringa, B. L.; Janssen, D. B. Versatile Peptide C-Terminal Functionalization via a Computationally Engineered Peptide Amidase. *ACS Catal.* **2016**, *6*, 5405−5414.
(25) Arnold, F. Engineering enzymes for non-aqueous solvents. *Trends Biotechnol.* **1990**, *8*, 244−249.
(26) Yu, H.; Huang, H. Engineering proteins for thermostability through rigidifying flexible sites. *Biotechnol. Adv.* **2014**, *32*, 308−315.
(27) Eijsink, V. G. H.; Bjørk, A.; Gåseidnes, S.; Sirevåg, R.; Synstad, B.; Burg, B. v. d.; Vriend, G. Rational engineering of enzyme stability. *J. Biotechnol.* **2004**, *113*, 105−120.
(28) Perutz, M. Electrostatic effects in proteins. *Science* **1978**, *201*, 1187−1191.
(29) Chen, J.; Yu, H.; Liu, C.; Liu, J.; Shen, Z. Improving stability of nitrile hydratase by bridging the salt-bridges in specific thermal-sensitive regions. *J. Biotechnol.* **2013**, *164*, 354−362.
(30) Zarrine-Afsar, A.; Zhang, Z.; Schweiker, K. L.; Makhatadze, G. I.; Davidson, A. R.; Chan, H. S. Kinetic consequences of native state optimization of surface-exposed electrostatic interactions in the Fyn SH3 domain. *Proteins* **2012**, *80*, 858.
(31) Lee, C.-F.; Makhatadze, G. I.; Wong, K.-B. Effects of Charge-to-Alanine Substitutions on the Stability of Ribosomal Protein L30e fromThermococcus celer†. *Biochemistry* **2005**, *44*, 16817.
(32) Steiner, K.; Schwab, H. Recent Advances in Rational Approaches for Enzyme Engineering. *Comput. Struct. Biotechnol. J.* **2012**, *2*, No. e201209010.
(33) Deuss, P. J.; Popa, G.; Botting, C. H.; Laan, W.; Kamer, P. C. J. Highly efficient and site-selective phosphane modification of proteins through hydrazone linkage: development of artificial metalloenzymes. *Angew. Chem., Int. Ed.* **2010**, *49*, 5315−5317.
(34) Haapalinen, A. M.; van Aalten, D. M.; Meriläinen, G.; Jalonen, J. E.; Pirilä, P.; Wierenga, R. K.; Hiltunen, J. K.; Glumoff, T. Crystal structure of the liganded SCP-2-like domain of human peroxisomal multifunctional enzyme type 2 at 1.75 Å resolution. *J. Mol. Biol.* **2001**, *313*, 1127−1138.
(35) van Leeuwen, P. W. N. M.; Casey, C. P.; Whiteker, G. T. *Phosphines as Ligands in Rhodium Catalysed Hydroformylation*; Van Leeuwen, P. W. N. M., Claver, C., Eds.; Kluwer Academic Publishers: New York, 2002; pp 63−105.
(36) van Leeuwen, P. W. N. M. *Rhodium Catalysed Hydroformylation in Homogeneous Catalysis, Understanding the Art*, Kluwer Academic Publishers: Dordrecht, 2004; pp 139−174.
(37) Bahrmann, H.; Bogdanovic, S.; van Leeuwen, P. W. N. M. *Higher Alkenes in Aqueous-Phase Organometallic Catalysis*; Cornils, B., Herrmann, W. A., Eds..; Wiley: Weinheim, 2004; pp 391−409.
(38) Joosten, H. J. Method of Generating a Protein database. WO2008035970 A3, 2008.
(39) Kourist, R.; Jochens, H.; Bartsch, S.; Kuipers, R.; Padhi, S. K.; Gall, M.; Böttcher, D.; Joosten, H.-J.; Bornscheuer, U. T. The α/β-Hydrolase Fold 3DM Database (ABHDB) as a Tool for Protein Engineering. *ChemBioChem* **2010**, *11*, 1635−1643.
(40) Lensink, M. F.; Haapalainen, A. M.; Hiltunen, J. K.; Glumoff, T.; Juffer, A. H. Response of SCP-2L Domain of Human MFE-2 to Ligand Removal: Binding Site Closure and Burial of Peroxisomal Targeting Signal. *J. Mol. Biol.* **2002**, *323*, 99−113.
(41) Filipp, F. V.; Sattler, M. Conformational Plasticity of the Lipid Transfer Protein SCP2. *Biochemistry* **2007**, *46*, 7980−7991.
(42) Berendsen, H. J. C. The α-helix dipole and the properties of proteins. *Nature* **1978**, *273*, 443−446.
(43) Armstrong, K. M.; Baldwin, R. L. Charged histidine affects alpha-helix stability at all positions in the helix by interacting with the backbone charges. *Proc. Natl. Acad. Sci. U.S.A.* **1993**, *90*, 11337.
(44) Carter, P. Site-directed mutagenesis. *Biochem. J.* **1986**, *237*, 1−7.
(45) Greenfield, N. J. Using circular dichroism collected as a function of temperature to determine the thermodynamics of protein unfolding and binding interactions. *Nat. Protoc.* **2006**, *1*, 2527−2535.
(46) Wijma, H. J.; Floor, R. J.; Jekel, P. A.; Baker, D.; Marrink, S. J.; Janssen, D. B. Computationally designed libraries for rapid enzyme stabilization. *Protein Eng. Des. Sel.* **2014**, *27*, 49−58.

https://dx.doi.org/10.1021/acscatal.0c05413
ACS Catal. 2021, 11, 3620−3627